

Article

Preparation of Nano- and Microparticles Obtained from Polymerization Reaction and Their Application to Surface Coating of Woody Materials

Toshinori Shimanouchi ^{1,*}, Daichi Hirota ¹, Masafumi Yoshida ¹, Kazuma Yasuhara ²  and Yukitaka Kimura ^{1,*}

¹ Department of Environmental Chemistry and Materials, Okayama University, 3-1-1 Tsushima-naka, Okayama 700-8530, Japan

² Division of Materials Science, Nara Institute of Science and Technology (NAIST), 8916-5 Takayama-cho, Ikoma 630-0192, Japan

* Correspondence: tshima@cc.okayama-u.ac.jp (T.S.); ykttkimu@cc.okayama-u.ac.jp (Y.K.)

Abstract: A surface coating of polymer particles of different hydrophobicity and wide-ranged size is helpful for the surface modification of materials such as woody thin board (WTB) derived from biomass. A preparation method for polymer particles was, in this study, proposed using a capillary-type flow system. Under hydrothermal conditions, the refinement of dispersed oil droplets in water (O/W emulsions) and the polymerization reaction could be simultaneously advanced, and polymer particles of polystyrene (PS), polyvinyl alcohol (PVA), polymethyl methacrylate (PMMA), and poly-L-lactic acid (PLLA) with a particle size of about 100 nm could be synthesized. The coating of polymer particles gave an improved effect on the water repellency of WTBs due to the hydrophobicity of polymer particles and an alteration of surface roughness, and it also provided long-term stability (more than 6 years).

Keywords: polymer particles; emulsification; water repellency; hydrophobicity; coating; convective self-assembly; wood thin board



Citation: Shimanouchi, T.; Hirota, D.; Yoshida, M.; Yasuhara, K.; Kimura, Y. Preparation of Nano- and Microparticles Obtained from Polymerization Reaction and Their Application to Surface Coating of Woody Materials. *Appl. Sci.* **2024**, *14*, 11326. <https://doi.org/10.3390/app142311326>

Academic Editor: Ana Martins Amaro

Received: 1 October 2024

Revised: 24 November 2024

Accepted: 27 November 2024

Published: 4 December 2024



Copyright: © 2024 by the authors. Licensee MDPI, Basel, Switzerland. This article is an open access article distributed under the terms and conditions of the Creative Commons Attribution (CC BY) license (<https://creativecommons.org/licenses/by/4.0/>).

1. Introduction

Cellulose and lignin are major components of lignocellulosic biomass [1–4]. A variety of applications of cellulose and lignin have progressed in terms of resource recycling [1,2]. The molecular conversion of cellulose and lignin into value-added compounds is a promising methodology to effectively use biomass [2–4]. Several useful chemical platforms from cellulose are glucose [5,6], fructose [5,6], 5-hydroxymethylfurfural [7], glycerol [8,9], lactic acid [8,9], and others [10,11], which are key compounds for C_n-chemistry. Furthermore, the use of cellulose has been advanced, i.e., cellulose-based materials including cellulose nanofiber [12–14], cellulose nanocrystalline [15], and cellulose derivatives [16]. Molecular conversion from lignin is also being vigorously studied.

Representative examples of cellulose-derived materials are cellulose (nano)fiber [12–14], cellulosic membranes for separation operation [17], reinforcing materials [13], labelled cellulose [18], and interfacial materials based on cellulose and lignin [16,19]. Block copolymers including cellulose have also been used to develop novel functional materials. For further improvement of the mechanical stability of cellulose- and polymer-based materials, lignin has been combined with them [12,16,19,20].

Cellulose-based interfacial materials have been designed in terms of rheological and chemical mechanical properties, as well as functionality [21]. Two representative interfacial materials based on cellulose are (i) a wood-plastic composite (WPC), which is a composite of woody materials with plastic, and (ii) plate-like materials obtained from the molding of a mixture of cellulose and lignin, which is called a woody thin board (WTB) [16,19]. WPC is the material obtained from woody biomass by a top-down approach, whereas WTB is

the material obtained from pure cellulose and lignin by a bottom-up approach. The surface property of WPC depends on the content and chain length of plastics (polymers) due to the entanglement between cellulose and polymer chains [22]. In contrast, lignin can modulate the interfacial property of WTBs such as hydrophobicity and water repellency [19]. Lignin can also act as a glue between cellulose beads to reinforce the mechanical stability of WTBs [16]. However, a high lignin content in a mixture of cellulose and lignin makes it impossible to form WTBs [16,19]. Therefore, the improved effect of water repellency in WTBs by lignin is limited to an increase from 45 deg to 60 deg [19].

As another approach, the chemical modification of cellulose by some chemical compounds has been examined: e.g., Ag nanoparticles [22] and diblock copolymers based on end-modified cellulose derivatives [16,20,23]. In our previous research, a dipping of poly-L-lactic acid (PLLA) could improve water repellency up to 80 deg [16]. For further improvement, PLLA-g-cellulose was synthesized by introducing PLLA into cellulose since PLLA is hydrophobic relative to cellulose. The use of PLLA-g-cellulose succeeded in the improvement of water repellency (water contact angle: 50 deg to 126 deg) by the orientation of PLLA-g-cellulose particles at the surface of WTB, because the chain of PLLA is an obstacle for burying in the grain boundary between cellulose particles [16]. On the other hand, the immersion of WTBs into the hydrophobic PLLA solution did not give higher hydrophobicity than the case using PLLA-g-cellulose [16]. However, the use of other hydrophobic polymers for the chemical modification of cellulose cannot always avoid the orientation into the grain boundary of cellulose particles, suggesting the need for alternative approaches.

As one method, surface modification using adhesion phenomena between polymer particles having various surface properties and cellulose particles is considered. However, there are few studies related to the cellulose/lignin-based material interface. In addition, in order to consider the partition of polymer particles into the grain boundaries formed by cellulose particles, it is necessary to control the polymer polymerization reaction to adjust the particle size from several tens of nanometers to several micrometers. For example, excellent preparation methods for polymer particles involve emulsion polymerization [24], suspension polymerization [25], and seed polymerization [26]. These methods are very useful for synthesizing particles of a size from 100 nm to several micrometers. However, it is difficult to produce polymer particles of several tens of nanometers. If an O/W emulsion of several tens of nanometers can be prepared from monomers, it is predicted that the desired fine particles can be prepared through suspension polymerization. We have previously reported that a hydrothermal emulsification method using a microcapillary provided the O/W emulsion with a size of at least 30 nm [27,28]. Therefore, combining the hydrothermal emulsification of a monomer with suspension polymerization is expected to yield polymer particles with the desired size.

In this study, we investigated the synthesis of polymer particles combining the hydrothermal emulsification of a monomer and suspension polymerization. Styrene, methyl methacrylate, vinyl acetate, and L-lactic acid were used. Environmentally friendly materials should be used for finishing WTBs. As is well known, L-lactic acid is biodegradable, but styrene and methyl methacrylate are not. However, the reason why we used styrene and methyl methacrylate with high hydrophobicity was that we considered that it is easy to verify whether it is possible to prepare polymer particles by hydrothermal emulsification and to investigate the effect of polymer hydrophobicity on surface modification, because their hydrophobicity, trend of entanglement, and softening properties largely differ from each other (Table 1). In addition, the reason is that these monomers can be easily polymerized by free-radical polymerization [25,26]. We examined whether the coating of WTBs with polymer particles could be controlled by these properties. The WTBs were obtained from a mixture of cellulose and lignin through a pressure molding method according to a previously described method [16,19] and modified with polymer particles. The surface state of WTBs treated by polymer particles was, with scanning electron microscopy (SEM) and atomic force microscopy (AFM), observed in terms of the convective assemblies of polymer

particles [29,30]. A water contact angle of WTBs coated with various polymer particles was measured to discuss the relationship between the water repellency and hydrophobicity. Furthermore, the long-term stability of WTBs was examined in terms of water contact angle and the ratio of cracked WTBs.

Table 1. Physical properties of polymers.

Polymer	Monomer	Hydrophobicity of Monomer, logP ^a	Entanglement Molecular Weight, M_e ^b	Softening Temperature, T_s [deg]
Polystyrene (PS)	styrene	2.95	18,700 ^c	~90
Poly(methyl methacrylate) (PMMA)	methyl methacrylate	1.38	9200 ^d	85–165
Poly(vinyl alcohol) (PVA)	vinyl alcohol	0.73	5100 ^e	85
Poly(lactic acid) (PLLA)	L-lactic acid	−0.62	9000 ^f	60–65

^a The logP value is the partition coefficient of a substrate in a biphasic octanol–water system [31]. ^b The M_e value was calculated using the equation $M_e = \rho RT / G_n^0$, where ρ is the density of the polymer, T is the measurement temperature of the storage modulus $G_n(\omega)$ of the melted polymers, R is the gas constant, and G_n^0 is the plateau value at the higher limit of the frequency range of $G_n(\omega)$ [32]. ^c [32,33]; ^d [34]; ^e [35,36]; ^f [37].

2. Materials and Methods

2.1. Materials

Purified lignin and cellulose (crystalline cellulose I) were purchased from Wako Pure Chemical Ltd. (Osaka, Japan). Styrene, methyl methacrylate, vinyl acetate, L-lactic acid, azobisisobutyronitrile (AIBN), and Tween 20 were purchased from Funakoshi Co. Ltd. (Tokyo, Japan). Other reagents were of analytical grade. A SUS316 tube, as a microcapillary (diameter 0.8 mm), and a SUS316 Tee connector were purchased from GL Sciences Inc. (Tsukuba, Ibaraki, Japan).

2.2. Polymerization Reaction Using Microcapillary

Styrene, methyl methacrylate, vinyl acetate, and lactic acid were used as the monomers of polymers. Their chemical structures are shown in Figure 1a. An O/W emulsion of nano-sized droplets was prepared by using a flow system as shown in Figure 1b [27,28]. The monomers with and without AIBN as the initiator of the radical polymerization reaction were suspended in water to form the oil-in-water (O/W) emulsion (Solution I). Afterwards, this Solution I was loaded with an HPLC pump (LC-20D, Shimadzu Corp., Kyoto, Japan), using a flow rate of 0.3 mL/min, into the oil bath (OHV-2000, EYELA, Tokyo, Japan) heated at 240 °C. Next, 0.0045 mM of Tween 20 solution (Solution II) was loaded with an HPLC-20AT (Shimadzu Corp., Kyoto, Japan) at 0.6 mL/min. Solutions I and II were mixed using a SUS Tee connector (GL Sciences) to stabilize the O/W emulsion. The flow rate ratio of Solutions I and II was initially 1:2. The flow rate ratio was changed to control the size of the O/W emulsion. A back pressure valve (P-880, Upchurch scientific, Tokyo, Japan) was used to keep a constant pressure of 10 MPa. The residence time that the liquid was heated at 240 °C in the oil bath was at most 4 min. The polymerization reaction of the monomer yielded the polymer suspension.

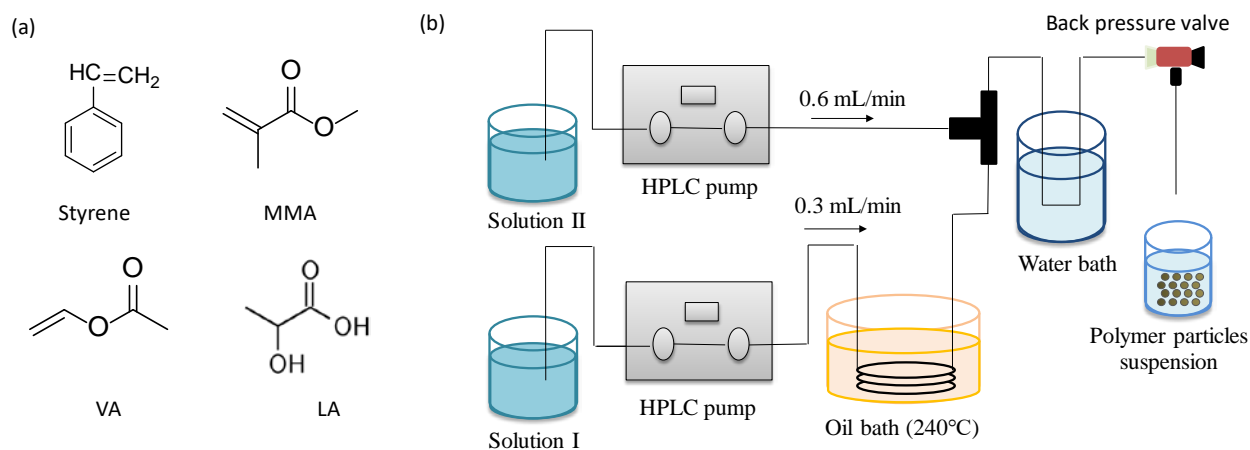


Figure 1. (a) Chemical structures of monomers used in this study. (b) Capillary-type flow system for emulsification. Solution I included monomer, AIBN, and Tween 20 (0.006 mM). Solution II was Tween 20 (0.0045 mM). Flow rate ratio of Solutions I and II was 1:2.

2.3. Preparation of WTBs by Compression Molding

WTBs were prepared according to previous reports [16,19]. Lignin and cellulose were mixed within a certain composition ratio for 20 min. An adequate amount of water was thereafter added to the mixture (30 mg) and milled for 2 min. The above mixture was injected into the metal mold, and compression molding was performed at 180 °C and 25 MPa for 10 min. Afterwards, the mold was considerably cooled down to recover WTBs with 10 mm × 10 mm in size and 0.3 mm in depth.

2.4. Immersion Method

First, the suspension of polymer particles was centrifuged with a rotation speed of 10,000 rpm for 30 min, and the subsequent removal of supernatants was performed to obtain the pellet of polymer particles. Thereafter, this pellet was resuspended in water to set the particle volume fraction (ϕ) to $\phi = 0.005$ and 0.020 . The suspension of polymer particles without any centrifugation indicated $\phi = 0.001$ – 0.005 . WTBs were horizontally immersed in a suspension including polymer particles. A subsequent drying process at 100 °C, which is greater than the softening temperature of lignin and the polymers used in this study, was performed for one day to improve the adhesion between the polymer particles and the surface of WTBs.

2.5. SEM Observation

The surface state of bare WTBs and WTBs immersed in polymer particles was observed by using SEM (S-4700, Hitachi Ltd., Tokyo, Japan). WTBs were mounted on metal stubs with double-faced tape, and images were taken. Prior to imaging, samples were coated with platinum–palladium in a sputter coater (E1030 Sputter, Hitachi Ltd.).

2.6. AFM Observation

An AFM (SPM9600, Shimadzu, Kyoto City, Japan) was also used at 25 °C for the same purpose. A silicon cantilever, OMCL-AC200TS (Olympus, Tokyo, Japan), which has a tetrahedral shape with a spring constant of 9 N/m and an oscillation frequency of 150 kHz, was used to scan the surface of the WTBs. The scan rate was 1 Hz. Scanning was performed at three different positions of each sample. The surface roughness was estimated with a root mean square average, R_{rms} . The R_{rms} value was calculated by using the equation $R_{\text{rms}} = (\sum y_i^2 / n)^{1/2}$, where the absolute values of the roughness profile y_i are ordinates [19].

2.7. Determination of Mean Diameter of Polymer Particles

The size distribution of polymer particles was measured using the dynamic light scattering mode of FPAR (Ohtsuka Electronics Co. Ltd., Osaka, Japan). The polydispersity

(PDI) of oil droplets was also estimated from the size distribution, by using cumulative analysis. The second-order auto-correlation function for measuring scattering light intensity, $G_2(\tau)$, is $G_2(\tau) = \langle I(t)I(t + \tau) \rangle / \langle I(t) \rangle^2$, where $I(t)$ is the scattering light intensity at time t and τ is the delay time. The auto-correlation function of polydispersed materials can be described as follows:

$$G_2(\tau) = A \left\{ 1 + B g_1^2(\tau) \right\}$$

$$g_1 = \int_0^{\infty} G(\Gamma) e^{-\Gamma \tau} d\Gamma$$

where A and B represent constants, and $g_1(\tau)$ represents the first-order auto-correlation function. $G(\Gamma)$ is the distribution function of the decay constant Γ . The mean value of Γ , $\langle \Gamma \rangle$, and the variance μ^2 are defined as follows.

$$\Gamma = \int_0^{\infty} \Gamma G(\Gamma) d\Gamma, \quad \mu^2 = \int_0^{\infty} (\Gamma - \langle \Gamma \rangle)^2 G(\Gamma) d\Gamma$$

Then, the PDI value can be defined as follows; a PDI < 0.1 signifies monodispersion.

$$\text{PDI} = \frac{\mu^2}{\Gamma}$$

2.8. Measurement of Contact Angle

The contact angle of water on the samples was measured by using an auto-contact angle/surface tensiometer (DSA 10, Krüss, Montreux, Switzerland). An aliquot of a water drop was poured onto the WTBS surface to sustain until the water drop did not move for at least 1 min. The image of the water drop was recorded and analyzed with data acquisition software (Model: Simage Standard 100 ver 1.01). Then, the contact angle was measured by drawing a line at the edge of the water drop. This measurement was performed three times per one WTBS.

2.9. Measurement of Long-Term Stability

A long-term stability experiment was performed according to a previous report [16]. In short, ten WTBSs were settled on a sheet at room temperature (20–27 °C, a relative humidity 20–30%). An aliquot of a water droplet was poured onto each WTBS every half year to measure the contact angle in the air. The contact angle was measured three times per one WTBS. Afterwards, the water droplet was eliminated by a piece of paper. WTBS cracking was ruled out to monitor the survival ratio of WTBSs. Then, the remaining WTBS [%] = $100 \times (10 - n) / 10$, where n is the number of cracked WTBSs. It was noted that the contact angle and remaining ratio of WTBSs were continuously measured as in previously published reports [16].

3. Results

3.1. Simultaneous Polymerization Reaction with Emulsification

In the first series of experiments, we prepared the polymer particles to improve the hydrophobicity of the WTBS surface. Three physicochemical properties are shown in Table 1. Styrene ($\log P = 2.95$), methyl methacrylate (MMA; $\log P = 1.38$), vinyl acetate (VA; $\log P = 0.73$), and L-lactic acid (LA; $\log P = -0.62$) were used as the monomers to give a change in hydrophobicity. The $\log P$ value, defined as a partition coefficient in biphasic octanol–water systems, represents the lipophilicity of chemical compounds (the affinity of a molecule for a lipophilic environment) [38], and a high $\log P$ value represents high hydrophobicity. The smaller the entanglement molecular weight (M_e) of the polymer, the more entangled it is. Since all polymers are below 18,700 g/mol, considerable entanglement is possible. Also, the softening temperature of each polymer (T_s) is also a useful index. A temperature below the T_s value is considered to be the surface condition of polymer particles for their adhesion. Therefore, the selected polymers in this study are considered to favor adhesion to WTBS surfaces.

3.1.1. Styrene

The formation of an O/W emulsion with styrene as a monomer was first attempted by using a capillary-type flow system. The O/W emulsion was then observed with cryogenic transmission electron microscopy (cryo-TEM). Figure 2a shows the successful formation of an O/W emulsion using styrene in the absence of AIBN. The contrast of a cryo-TEM image depends on the electron density of the chemical compounds [39]. Since styrene bears a benzene ring with rich electron density, the oil (styrene) phase gave high contrast to the water phase. Thus, the use of the capillary-type flow system under hydrothermal conditions made it possible to yield an O/W emulsion of styrene, as well as typical oil phases such as decane and octanoic acid [28,29].

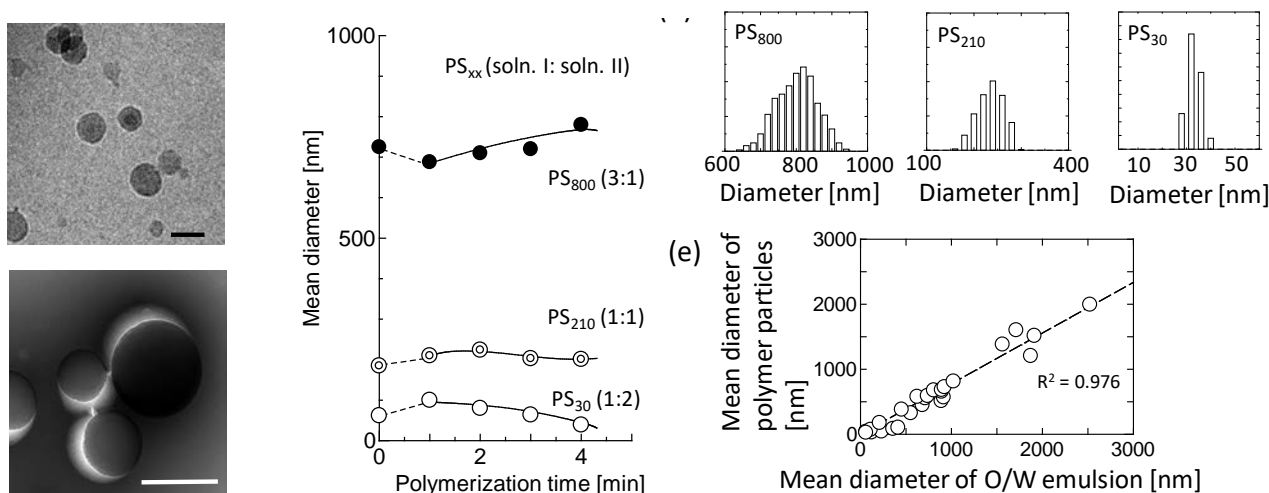


Figure 2. (a) Cryo-TEM images of O/W emulsion of styrene. (b) TEM image of nanoparticles made of PS. (c) Time course of mean diameter for PS particles. Samples at $t = 0$ and $t > 0$ represent O/W emulsion without AIBN and after polymerization reaction, respectively. (d) Diameter distribution of PS₈₀₀, PS₂₁₀, and PS₃₀. (e) Comparison of diameter of O/W emulsion with that of polymer particles. PS_{xx} indicates PS with xx nm of final mean diameter.

The formation of polymer particles is considered to be driven by the hydrothermal emulsification of an O/W emulsion in the presence of the polymerization initiator AIBN. Typical TEM images are shown in Figure 2b. A polystyrene particle, dispersed in water, was observed. The diameter of polystyrene particles was indicated to be 100–200 nm. The size dependency of polymer particles was next examined by altering the initial size of the O/W emulsion. The flow rate of Solution II was altered while keeping the flow rate of Solution I (0.30 mL/min) to control the size change of the O/W emulsion. A flow rate ratio of Solutions I and II = 1:2 yielded the minimum size of the emulsion without AIBN (58–120 nm). The larger flow rate ratio favored the large mean diameter of the O/W emulsion. Fixing the flow rate ratio of Solutions I and II (1:2), the polymerization reaction of O/W emulsions with different sizes were then monitored as a function of the polymerization time (Figure 2c). In the case of the O/W emulsion with 100 to 200 nm of diameter, the mean diameter of polystyrene (PS) particles slightly altered into 30 and 210 nm, respectively. Polystyrene particles of a mean diameter of r nm were termed PS _{r} . The size distribution of PS₃₀, PS₂₁₀, and PS₈₀₀ indicated a single peak (Figure 2d). The mean diameter of the O/W emulsion was roughly correlated with that of the polymer particles, as shown in Figure 2e. Therefore, the O/W emulsion was likely to act as the template for the formation of polymer particles. The final size of the polymer particles was likely to be controlled by the flow rate ratio of Solutions I and II.

3.1.2. Other Monomers

VA, MMA, and LA were used as monomers. The O/W emulsions were observed (black arrows in Figure 3a). Small aggregates other than the O/W emulsion were likely to be a frost generated during the setting of the cryo-sample into the TEM chamber, from the previous study [40]. The addition of AIBN induced a polymerization reaction as well as styrene. Figure 3b indicated the formation of polymer particles using these monomers. Figure 3c shows the typical result of the time-course of the diameter in the polymerization process. The increase in particle size is attributed to adhesion by the entanglement between the polymer particles. On the other hand, PMMA tended to decrease, which may be due to the removal of water from the polymer particles during the polymerization reaction. It is noted that there was sometimes a blockage in the microcapillary during the polymerization of LA. Furthermore, a rough correlation between the mean diameter of the O/W emulsion without AIBN and that of polymer particles was observed (Figure 3d), which is in agreement with Figure 2e. Therefore, O/W emulsions of VA, MMA, and LA also appeared to act as templates for polymer particles, as well as styrene.

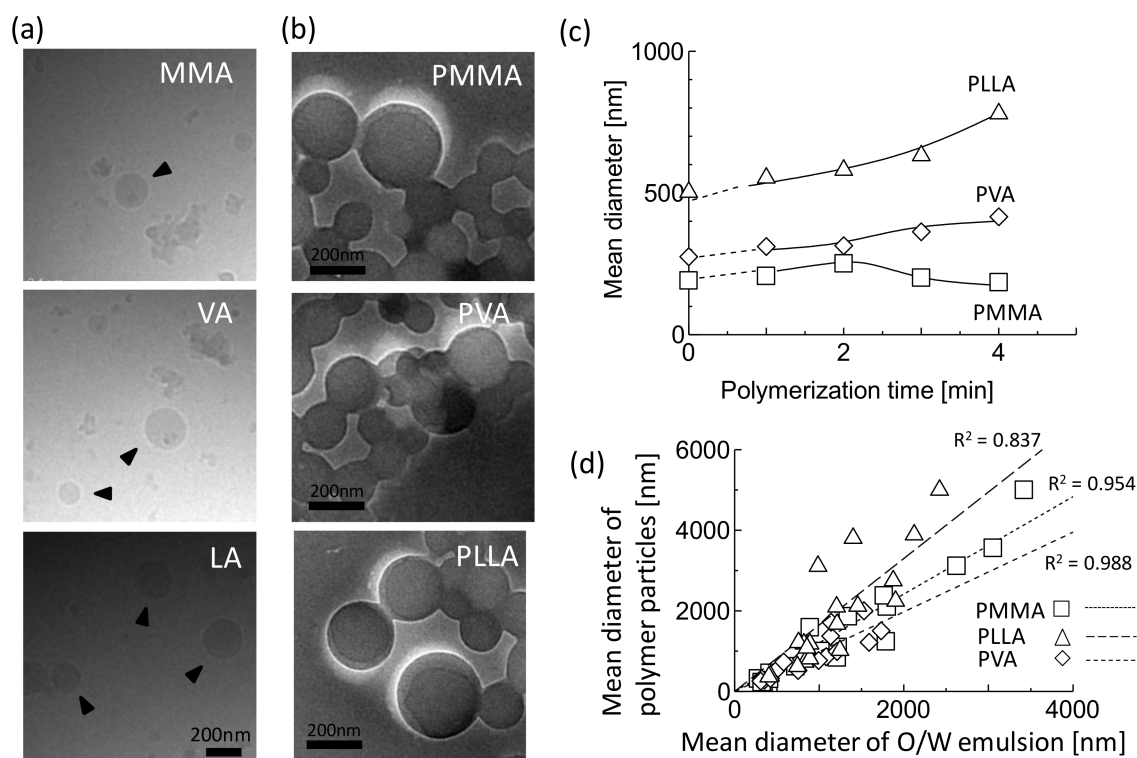


Figure 3. (a) Cryo-TEM images of O/W emulsions of MMA, VA, and LA. Black arrows represent O/W emulsion. (b) TEM images of polymer particles made of PMMA, PVA, and PLLA. (c) Typical time-course of polymerization of O/W emulsions. Flow rate ratio of Solutions I (0.30 mL/min) and II (0.60 mL/min) was 1:2. (d) Comparison of diameter of O/W emulsion with that of polymer particles.

3.2. Coatings by Polymer Particles

WTBs were first prepared by using compression molding (see Section 2.3). Coating with polymer particles was thereafter performed on the WTBs. Our previous study demonstrated that the microfibrillar structure of cellulose I exists on the surfaces of WTBs, and that lignin favors remaining on the surface. [19]. The composition ratio of the ternary lignin/cellulose/water system to prepare the WTBs was selected to have the highest value of the water contact angle, an index of water repellency, according to our previous study [16].

3.2.1. Surface Observation

Surface observation using SEM and AFM gives qualitative information about the coating of polymer particles on WTBs [19]. We observed the surfaces of WTBs to confirm the influence of physical modification with polymer particles, by using SEM. The surfaces of bare WTBs were then observed (Figure 4a). The microfibrillar structures of cellulose I were observed. The surface roughness of the bare WTBs indicated $R_{\text{rms}} = 114 \text{ nm}$, which is in agreement with the literature [19].

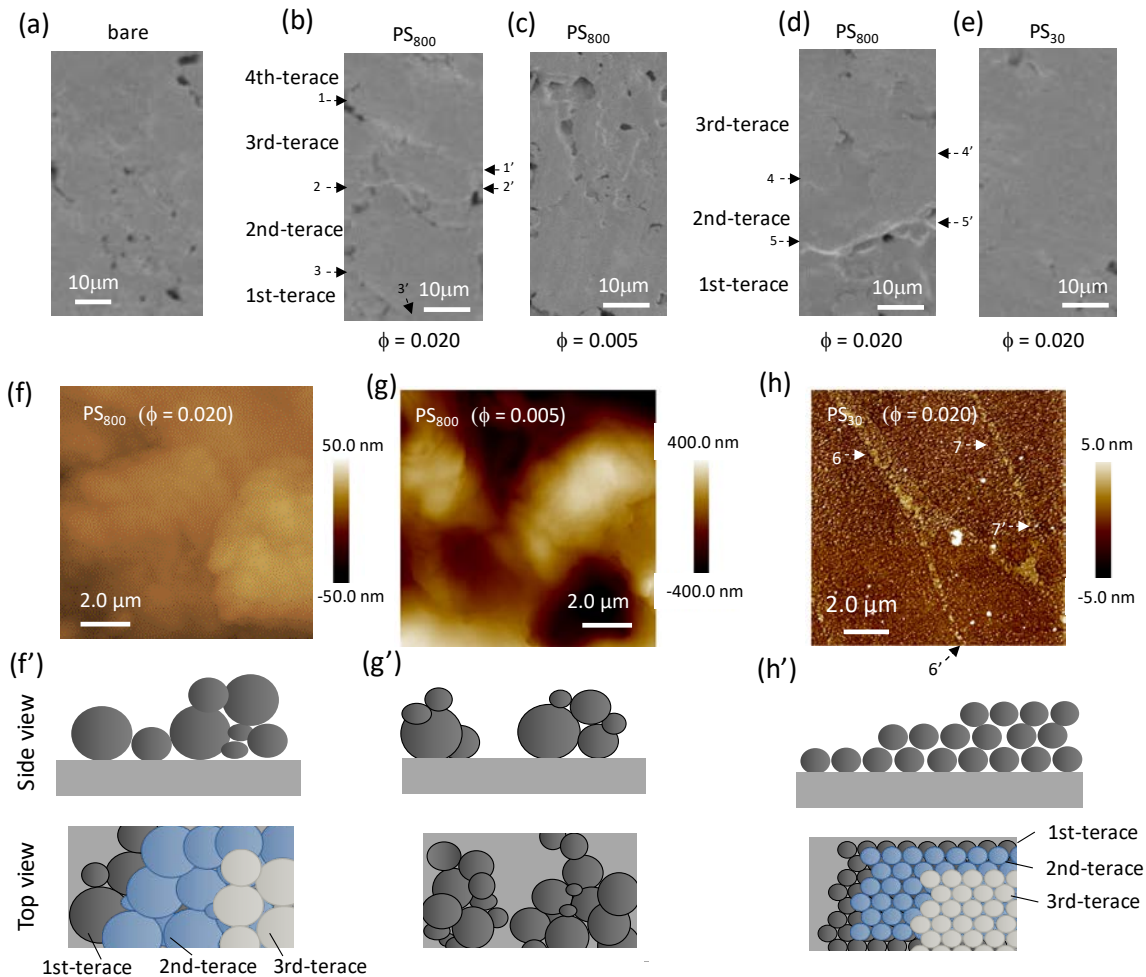


Figure 4. (a–e) SEM and (f–h) AFM images of bare WTB and WTBs coated by polystyrene particles with different diameters at two volume fractions ($\phi = 0.005$ and 0.020). (f'–h') Both side and top views of each AFM image. White and black arrows mean the step on the surface. Lines 1–1', 2–2', ... and 7–7' mean the step.

First, the effect of the volume fraction of polymer particles on the surface structure of WTBs was examined. The surfaces of WTBs immersed in PS_{800} were compared by using $\phi = 0.020$ and 0.005 . The surface obtained in the case of $\phi = 0.020$ involved steps like 1–1', 2–2', and 3–3', and four layers (four terraces) between the steps were observed, which was similar to the formation of a multilayered deposition of latex particles (polystyrene) [29,30]. In contrast, the surface obtained from immersion in PS_{800} at $\phi = 0.005$ gave no definite terrace on the surface (Figure 4c). Therefore, the volume fraction of the polymer particles made an impact on the surface. Alternatively, regarding the effect of the mean diameter of the polymer particles, the surface states of WTBs were compared with $\phi = 0.020$. The surface in the case of PS_{30} (Figure 4e) gave no definite terrace structure different from PS_{800} (steps 4–4' and 5–5' in Figure 4d). The formation of terraces appeared to depend on the size and volume fraction of the polymer particles.

For further investigation, AFM observation was performed. The surfaces of WTBs immersed in PS₈₀₀ at $\phi = 0.020$ indicated a conspicuous undulating structure of $R_{\text{rms}} = 83.5$ nm (Figure 4f). This surface morphology might result from the terrace structure as illustrated in Figure 4f'. Decreasing ϕ to 0.005, the AFM image showed a clear undulating structure of $R_{\text{rms}} = 531$ nm (Figure 4g), which possibly resulted from the exposure of bare WTBs. It was likely that PS₈₀₀ could not considerably coat the WTB surfaces (Figure 4g'). Furthermore, in contrast to PS₈₀₀ at $\phi = 0.020$, the size of the PS decreased to 30 nm. Thereby, the AFM image of the surfaces of WTBs immersed in PS₃₀ at $\phi = 0.020$ indicated a terrace structure at the nanoscale of $R_{\text{rms}} = 18.1$ nm (steps 6–6' and 7–7' in Figure 4h,h'), although no definite terrace structure at the microscale was observed (Figure 4e). It is noted that the R_{rms} value strongly depends on the bare WTB surface before adhesion.

3.2.2. Water Repellency

The water contact angle under the air condition was measured to evaluate the influence of terrace formation on the WTB surface. In the case of water droplets used as liquid droplets, the contact angle, θ , is considered the index of water repellency. Figure 5 shows the contact angle for each board immersed in each polymer at $\phi = 0.005$ and 0.020. Bare boards had the smallest contact angles (55 deg) of the boards tested here. Overall, coating the WTBs improved water repellency, especially in the case of PS-, -PMMA-, and PVA-particles.

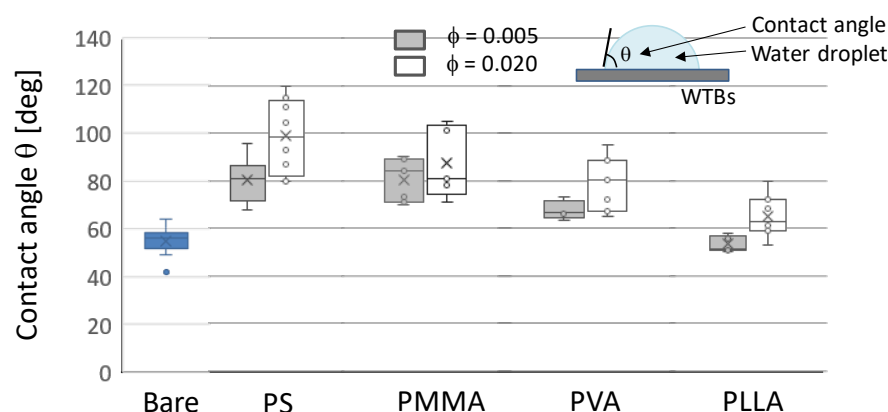


Figure 5. Box plots of contact angles for WTBs coated by polymer particles at two ϕ values. “Bare” means the WTB without surface modification of polymer particles.

3.2.3. Comparison of Polymer Particles on Water Repellency

The water repellency depended on the surface roughness to some extent [19]. From Figure 4, the surface roughness resulted from the coating of polymer particles with different size. Accordingly, the water repellency was compared with the size of the polymer particles. Any contact angle surpassed that of bare WTBs, regardless of the ϕ value (Figure 6). The water contact angle was negatively correlated with the size of the polymer particles at $\phi = 0.020$. The contact angle at $\phi = 0.020$ was fitted to an exponential relaxation: $\theta = \theta_{\text{limit}} + (\theta_{\text{limit}} - \theta_{\text{bare}})e^{-d/D}$, where d , D , θ_{bare} , and θ_{limit} are the mean size of the polymer particles, a constant, the contact angle for bare WTBs, and the contact angle estimated at $d = 0$, respectively. The θ_{limit} value is also termed the contact angle limit. The θ_{limit} value was proportional to the $\log P$ value for each monomer (Figure 6e), suggesting water repellency depended on the hydrophobicity of the polymers. In the case of PS, PMMA, and PVA, the improved effect of water repellency using polymer particles was higher than those using polymer membranes (dipping). The same was true for the plastic surface of each polymer. In contrast, in the case of PLLA, its polymer particles had water repellency comparable to its polymer membranes. From the rough surface of the PLLA membrane, these results suggested that the improved effect of water repellency resulted not only from the hydrophobicity of polymers but also from the surface roughness.

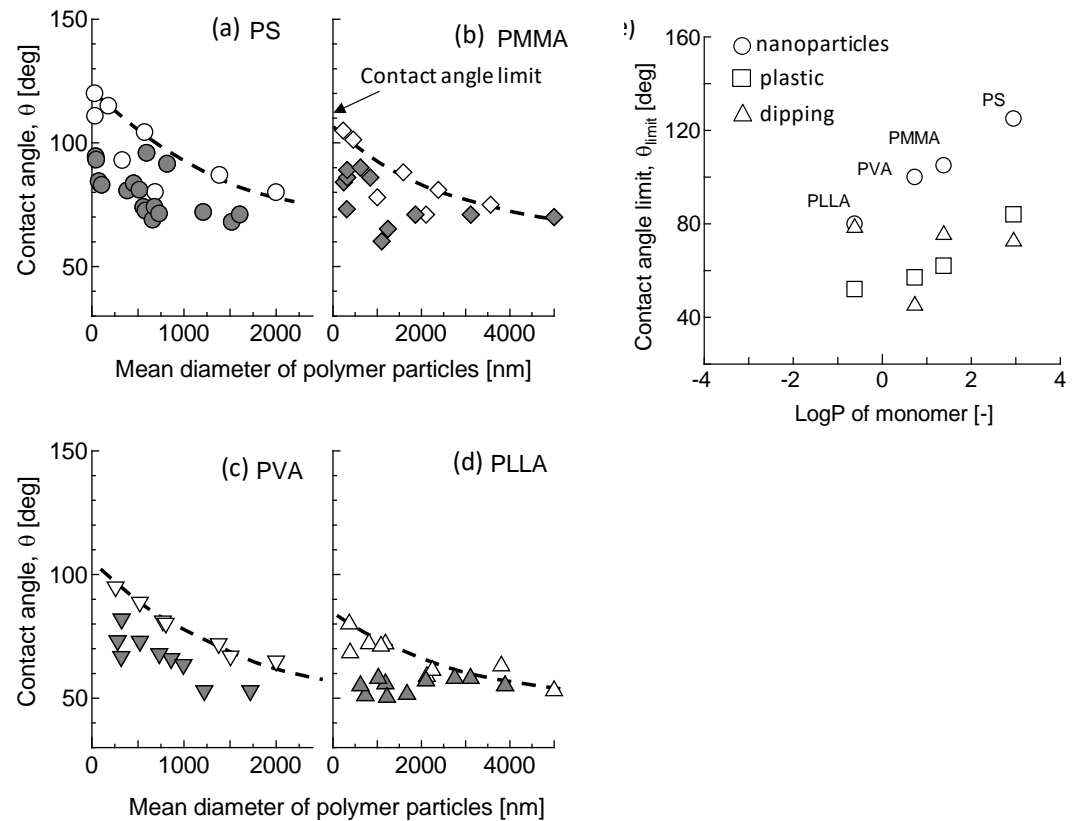


Figure 6. A comparison of the contact angle of the WTB surface with the mean diameter of the polymer particles: (a) PS; (b) PMMA; (c) PVA; and (d) PLLA. White and gray keys represent WTBs modified at $\varphi = 0.020$ and 0.005 , respectively. (e) The relationship between the contact angle limit of WTBs and $\log P$ values for each monomer. Dashed curve in (a–d) is a curve fitted with exponential relaxation.

3.3. Long-Term Stability

A comparison of surface modifications of WTBs with PSs of different mean diameters was examined. Figure 7a shows the long-term stability concerning water repellency. Initially, the contact angle was 120 deg, 105 deg, and 93 deg for PS₃₀-, PS₅₁₅-, and PS₈₀₀-coated WTBs, respectively. PS₅₁₅- and PS₈₀₀-coated WTBs indicated a decrease in water repellency and eventually the same level as bare WTBs (53 deg). In contrast, PS₃₀-coated WTBs indicated a constant contact angle (120 deg). Therefore, the long-term stability depended on the mean diameter of the PS.

Next, the effect of the hydrophobicity of the polymer on long-term stability was examined. In this trial, polymer particles with 30–50 nm of diameter were used. A coating of PS₃₀ indicated the highest value of the contact angle of polymers. The water repellency for PS- and PMMA-coated WTBs and bare WTB remained almost constant for six years. The PVA- and PLLA-coated WTBs indicated a slight reduction in water repellency (Figure 7b).

Together with this, the survival of WTBs is monitored in Figure 7c. First, the order of decremental numbers of WTBs was bare > PLLAs > PVAs > PMMA > PS. Second, 90%, 80%, 60%, 60%, and 30% of WTBs coated with PS, PMMA, PVA and PLLA and bare WTBs survived more than six years, respectively.

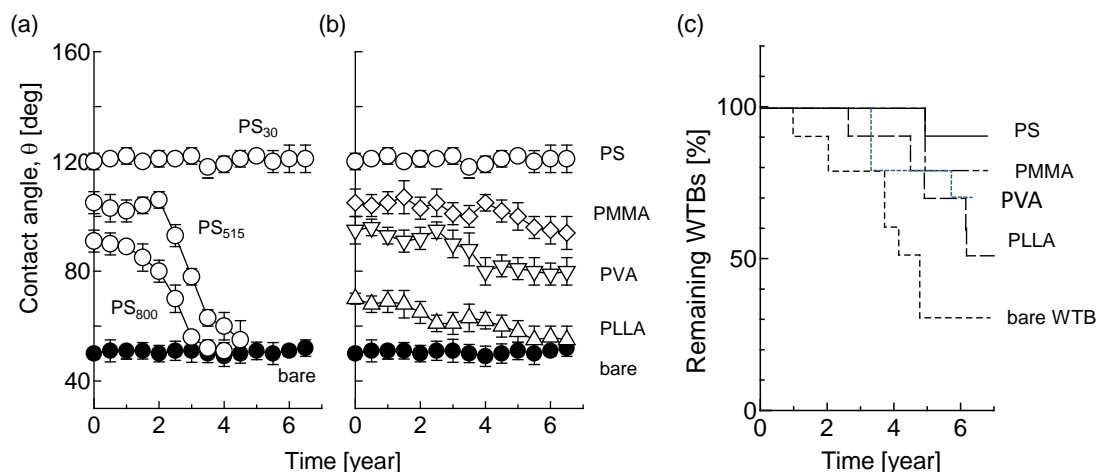


Figure 7. Long-term stability of WTBs. (a) WTBs modified with PS of different diameters and (b) four kinds of polymer particles. (c) Remaining ratio of WTBs. Initially, ten WTBs were prepared. Standard errors were calculated from four different experiments for each WTB.

Thus, the coating of WTBs with polymer particles gave an impact on not only water repellency but also the stability of the WTBs. The water repellency depended on the diameter of the polymer particles and the logP value of the monomers.

4. Discussion

In this study, hydrothermal emulsification allowed us to form an O/W emulsion made of a monomer to obtain polymer particles initiated through a polymerization reaction by AIBN. The size of O/W emulsion was comparable to the size of the polymer particles, for which the O/W emulsions acted as the template. Thereafter, the coating of WTBs was tested by using the polymer particles. The size of the polymer particles likely determined the water repellency, as well as the hydrophobicity at the surface, which is herein discussed.

The size control of the polymer particles is first discussed. As mentioned in Section 3.1.1, the final size of the polymer particles was likely to be affected by the flow rate ratio of Solutions I and II. This was because of the controllable size distribution of O/W emulsions as a template for the polymer particles, as shown in Figure 2e). 2D simulations giving the velocity vector around the T-junction [41] demonstrated that the fluid was squeezed by the strong shear stress occurring at the surface of the fluid injected through the T-junction. The strength of the vortex field depended on the flow rate ratio of Solutions I and II. A large flow rate ratio such as 1:3 and 1:4 might induce weak shear stress around the T-junction, making the O/W emulsion reduce its size.

The size of the polymer particles can qualitatively affect the surface roughness (Figure 4). The formation of terraces on the surface enables us to give the surface roughness. From the plots of the mean diameter of the polymer particles and their contact angles (Figure 6a–d), a coating of polymer particles of small size was subject to yield a high contact angle; i.e., the contact angle limit of WTBs coated by polymer particles was strongly correlated with the hydrophobicity of the monomer (logP value), as shown in Figure 6e. However, the correlation in Figure 6e depends on the method of surface modification. This resulted from the hydrophobicity of the polymers used as polymer particles. Alternatively, a decrease in the size of the polymer particles elevated the contact angle up to 120 deg, regardless of the type of polymer, strongly suggesting the contribution to the contact angle of the surface roughness originated from the polymer particles adsorbed on the surface of the WTBs. It is noted that the contact angle should be, ideally, negatively correlated with the surface roughness [42,43].

Next, how the surface roughness of WTBs coated with polymer particles was generated is discussed. As seen in Figure 4, PS₃₀ gave a flattened surface as compared with the surface coated by PS₈₀₀. This trend was in agreement with a report that a coating of polystyrene latex particles with diameters of 309 and 2106 nm induced smooth and rough surfaces, respectively [29]. The softening temperature of polymers, T_s , is also a key factor. The T_s value for each polymer is

summarized in Table 1. The drying temperature for a coating of WTBs with polymer particles was set 100–120 °C, which was higher than that of lignin ($T_s \sim 60$ °C) and lower than that of cellulose ($T_s \sim 240$ °C). The T_s values for the polymers used in this study were lower than the drying temperature, as seen in Table 1. It was considered that polymers other than cellulose became softened during the drying process. It was considered that the convective self-assembly of polymer particles occurred in the drying process. The dispersion state originating from the convective self-assembly appeared to depend on the volume fraction of the polymer particles (Figure 4f–h). Convective self-assembly resulting from polymer–polymer and polymer–lignin (or cellulose) adhesion might be induced due to the entanglement of the polymers. As the size of polymer particles became smaller, the surface became more smooth, as shown in Figure 4e,h.

If the size of the polymer particles was extrapolated to zero, the contact angle limit estimated in Figure 6a–d was proportional to the hydrophobicity (Figure 6e). Even in the case of PS-coated WTBs, the contact angle limit was 125 deg. This value was lower than the superhydrophobicity (161 deg) achieved by a PS-tuned thermoplastic surface based on the annealing temperature [44]. Also, the fine roughness gives superhydrophobicity with a high contact angle, which is called the lotus effect or petal effect [32,45]. Other surface states based on dipping and plastic gave contact angles lower than the corresponding contact angle limit. It was therefore suggested that the improvement of water repellency requires not only hydrophobicity but also the surface morphology to exert the lotus effect and petal effect. If so, the correlation between the contact angle limit and logP in Figure 6e can be regarded as the boundary of the contribution to hydrophobicity and surface roughness.

Finally, the long-term stability of polymer particle-coated WTBs (Figure 7) is discussed. The adhesion of polymer particles based on their entanglements was considered to contribute to the improved effect of the long-term stability of WTBs. For long-term stability, PLLA-coated WTBs indicated the fewest remaining WTBs among the tested ones (Figure 7c). Mathew et al. have reported that microcrystalline cellulose indicated poor adhesion with PLLA [32]. The water repellency of PLLA-coated WTBs and their remaining WTBs in the long term (Figure 7b,c) can be then attributed to their poor adhesion property. From the aforementioned discussion, it was considered that the softening of polymer particles at a temperature above T_s during coating favored entanglement enough to stabilize the adhesion of polymer particles to WTB surfaces.

5. Conclusions

It is likely that the use of a capillary-type flow system under hydrothermal conditions allowed us to form a finely dispersed O/W emulsion. Furthermore, a simultaneous polymerization reaction over the emulsification provided polymer particles with less than 30 nm in diameter. Thus, the combination of hydrothermal emulsification and polymerization made it possible to yield polymer particles. These polymer particles gave an improved effect on water repellency (contact angle limit ~ 120 deg) as compared with the bare WTB (50 deg). The present improved effect of water repellency resulted mainly from the hydrophobicity of the polymer particles. Interestingly, a terrace-like surface was observed, which probably resulted from the convective self-assembly of polymer particles on the WTB surface. Finally, the coating of polymer particles above the softening temperature was useful for the improved effect of water repellency and long-term stability. The present findings give better insight into the design of functional and environmentally benign polymers and the convective self-assembly of polymer colloidal particles on solid surfaces.

Author Contributions: Conceptualization, T.S.; methodology, T.S.; formal analysis, D.H.; investigation, D.H., M.Y. and K.Y.; data curation, D.H. and M.Y.; writing—original draft preparation, T.S.; writing—review and editing, T.S., K.Y. and Y.K.; supervision, T.S. and Y.K.; funding acquisition, T.S. All authors have read and agreed to the published version of the manuscript.

Funding: This research was also supported by the Yakumo Foundation (in the fiscal year 2016) for the preparation of PLLA.

Institutional Review Board Statement: Not applicable.

Informed Consent Statement: Not applicable.

Data Availability Statement: The datasets presented in this article are not readily available because the data are part of an on-going study on the long-term stability of WTBs.

Acknowledgments: The authors thank Sakiko Fujita for her technical support concerning cryo-TEM and TEM observation.

Conflicts of Interest: The authors declare no conflicts of interest.

References

1. Mankar, A.R.; Pandey, A.; Modak, A.; Pant, K.K. Pretreatment of lignocellulosic biomass: A review on recent advances. *Biores. Technol.* **2021**, *334*, 125235. [[CrossRef](#)]
2. Ashokkumar, V.; Venkatkarthick, R.; Jayashree, S.; Chuetor, S.; Dharmaraj, S.; Kumar, G.; Chen, W.-H.; Ngamcharussrivichai, C. Recent advances in lignocellulosic biomass for biofuels and value-added bioproducts—A critical review. *Biores. Technol.* **2022**, *344*, 126195. [[CrossRef](#)] [[PubMed](#)]
3. Wu, H.; Zhang, R.; Zhai, Y.; Song, X.; Xiong, J.; Li, X.; Qiano, Y.; Lu, X.; Yu, Z. Solvent effects enable efficient tandem conversion of cellulose and its monosaccharides towards 5-hydroxymethylfurfural. *ChemSusChem* **2023**, *16*, e202201809. [[CrossRef](#)] [[PubMed](#)]
4. Millán, G.G.; Hellsten, S.; Llorca, J.; Luque, R.; Sixta, H.; Balu, A.M. Recent advances in the catalytic production of platform chemicals from holocellulosic biomass. *ChemCatChem* **2019**, *11*, 2022–2042. [[CrossRef](#)]
5. Moller, M.; Harnisch, F.; Schrader, U. Microwave-assisted hydrothermal degradation of fructose and glucose in subcritical water. *Biomass Bioenergy* **2012**, *39*, 389–398. [[CrossRef](#)]
6. Song, B.; Wu, Z.; Yu, Y.; Wu, H. Hydrothermal Reactions of Biomass-Derived Platform Molecules: Distinct Effect of Aprotic and Protic Solvents on Primary Decomposition of Glucose and Fructose in Hot-Compressed Solvent/Water Mixtures. *Ind. Eng. Chem. Res.* **2020**, *59*, 7336–7345. [[CrossRef](#)]
7. Wu, Z.; Yu, Y.; Wu, H. Hydrothermal Reactions of Biomass-Derived Platform Molecules: Mechanistic Insights into 5-Hydroxymethylfurfural (5-HMF) Formation during Glucose and Fructose Decomposition. *Energy Fuels* **2023**, *37*, 2115–2126. [[CrossRef](#)]
8. Akbukut, D.; Ozkar, S. A review of the catalytic conversion of glycerol to lactic acid in the presence of aqueous base. *RSC Adv.* **2022**, *12*, 18864–18883. [[CrossRef](#)]
9. Shimanouchi, T.; Takahashi, Y.; Yasuhara, K.; Kimura, Y. Conversion of glycerol to lactic acid by using platinum-supported catalyst combined with phosphatidylcholine vesicles. *Chem. Lett.* **2023**, *52*, 426–429. [[CrossRef](#)]
10. Weigarten, R.; Cho, J.; Conner, C., Jr.; Huber, G.W. Kinetics of furfural production by dehydration of xylose in a biphasic reactor with microwave heating. *Green Chem.* **2012**, *12*, 1423–1429. [[CrossRef](#)]
11. Chen, C.; Wang, L.; Zhu, B.; Zhou, Z.; El-Hout, S.I.; Yang, J.; Zhang, J. 2,5-Furandicarboxylic acid production via catalytic oxidation of 5-hydroxymethylfurfural: Catalysts, processes and reaction mechanism. *J. Energy Chem.* **2021**, *54*, 528–554. [[CrossRef](#)]
12. Bian, H.; Wei, L.; Lin, C.; Ma, Q.; Dai, H.; Zhu, J.Y. Lignin-Containing Cellulose Nanofibril-Reinforced Polyvinyl Alcohol Hydrogels. *ACS Sustain. Chem. Eng.* **2018**, *6*, 4821–4828. [[CrossRef](#)]
13. Okahisa, Y.; Matsuoka, K.; Yamada, K.; Wataoka, I. Comparison of polyvinyl alcohol films reinforced with cellulose nanofibers derived from oil palm by impregnating and casting methods. *Carbohydrate Polym.* **2020**, *250*, 116907. [[CrossRef](#)] [[PubMed](#)]
14. Ueda, T.; Ishigami, A.; Thumsorn, S.; Kurose, T.; Kobayashi, Y.; Ito, H. Structural, rheological, and mechanical properties of polyvinyl alcohol composites reinforced with cellulose nanofiber treated by ultrahigh-pressure homogenizer. *Mater. Today Commun.* **2022**, *33*, 104316. [[CrossRef](#)]
15. Heise, K.; Delepierre, G.; King, A.W.T.; Kostianen, M.A.; Zoppe, J.; Weder, C.; Kontturi, E. Chemical Modification of Reducing End-Groups in Cellulose Nanocrystals. *Angew. Chem. Int. Ed.* **2021**, *60*, 66–87.
16. Shimanouchi, T.; Yoshida, M.; Yang, W.; Kimra, Y. Effect of cellulose-g-poly(L-lactide) on the properties of woody thin boards made of lignin/cellulose biphasic system: Water repellency and long-term stability. *Poly. Sci. Peer Rev. J.* **2021**, *3*, 536–542.
17. Rana, A.K.; Gupta, V.K.; Saini, A.K.; Voicu, S.I.; Abdellattifaand, M.H.; Thakur, V.K. Water desalination using nanocelluloses/cellulose derivatives based membranes for sustainable future. *Desalination* **2021**, *520*, 115359. [[CrossRef](#)]
18. Kim, N.H.; Imai, T.; Wada, M.; Sugiyama, J. Molecular Directionality in Cellulose Polymorphs. *Biomacromolecules* **2006**, *7*, 274–280. [[CrossRef](#)]
19. Shimanouchi, T.; Kamba, T.; Yang, W.; Aoyagi, S.; Kimura, Y. Surface properties of woody thin boards composed of commercially available lignin and cellulose: Relationship between the orientation of lignin and water repellency. *Appl. Surf. Sci.* **2015**, *347*, 406–413. [[CrossRef](#)]
20. Nakagawa, A.; Steiniger, F.; Richter, W.; Koschella, A.; Heinze, T.; Kamitakahara, H. Thermoresponsive Hydrogel of Diblock Methylcellulose: Formation of Ribbonlike Supramolecular Nanostructures by Self-Assembly. *Langmuir* **2012**, *28*, 12609–12618. [[CrossRef](#)]
21. Barhoum, A.; Rastogi, V.K.; Mahur, B.K.; Rastogi, A.; Abdel-Haleem, F.M.; Samyn, P. Nanocelluloses as new generation materials: Natural resources, structure-related properties, engineering nanostructures, and technical challenges. *Mater. Today Chem.* **2022**, *26*, 101247. [[CrossRef](#)]

22. Martins, N.C.T.; Freire, C.S.R.; Pinto, R.J.B.; Fernandes, S.C.M.; Pascoal Neto, C.; Silvestre, A.J.D.; Causio, J.; Baldi, G.; Sadocco, P.; Trindade, T. Electrostatic assembly of Ag nanoparticles onto nanofibrillated cellulose for antibacterial paper products. *Cellulose* **2012**, *19*, 1425–1436. [[CrossRef](#)]
23. Kamitakahara, H.; Enomoto, Y.; Hasegawa, C.; Nakatsubo, F. Synthesis of Diblock Copolymers with Cellulose Derivatives. 2. Characterization and Thermal Properties of Cellulose Triacetate-Block-Oligoamide-15. *Cellulose* **2005**, *12*, 527–541. [[CrossRef](#)]
24. Kong, D.C.; Yang, M.H.; Zhang, X.S.Z.; Du, C.; Fu, Q.; Gao, X.Q.; Gong, J.W. Control of Polymer Properties by Entanglement: A Review. *Macromol. Mater. Eng.* **2021**, *306*, 2100536. [[CrossRef](#)]
25. Lovell, P.A.; Schork, F.J. Fundamentals of emulsion polymerization. *Biomacromolecules* **2020**, *21*, 4396–4441. [[CrossRef](#)] [[PubMed](#)]
26. Nagao, D.; Hashimoto, M.; Hayasaka, K.; Konno, M. Synthesis of anisotropic polymer particles with soap-free emulsion polymerization in the presence of a reactive silane coupling agent. *Macromol. Rapid Commun.* **2008**, *29*, 1484. [[CrossRef](#)]
27. Shimanouchi, T.; Tange, T.; Kimura, Y. Subcritical water-assisted emulsification of decane/water: Influence of surfactants. *Solvent Extr. Res. Dev. Jpn.* **2014**, *21*, 103–110. [[CrossRef](#)]
28. Shimanouchi, T.; Tange, T.; Kimura, Y. Subcritical Water-Assisted Emulsification of Oil/Water: The Effect of Solubility of Organic Solvent and Surfactants. *Solvent Extr. Res. Dev. Jpn.* **2014**, *21*, 223–230. [[CrossRef](#)]
29. Prevo, B.G.; Velev, O.D. Controlled, rapid deposition of structured coatings from micro- and nanoparticle suspensions. *Langmuir* **2004**, *20*, 2099–2107. [[CrossRef](#)]
30. Dimitrov, A.S.; Nagayama, K. Continuous convective assembling of fine particles into two-dimensional arrays on solid surfaces. *Langmuir* **1996**, *12*, 1303–1311. [[CrossRef](#)]
31. Mathew, A.P.; Oksman, K.; Sain, M. Mechanical properties of biodegradable composites from poly lactic acid (PLA) and microcrystalline cellulose (MCC). *J. Appl. Poly. Sci.* **2005**, *97*, 2014–2025. [[CrossRef](#)]
32. Ferry, J.D. *Viscoelastic Properties of Polymers*; Wiley: New York, NY, USA, 1980.
33. Santangelo, P.G.; Roland, C.M. Molecular Weight Dependence of Fragility in Polystyrene. *Macromolecules* **1998**, *31*, 4581–4585. [[CrossRef](#)]
34. Wu, S. Chain structure and entanglement. *J. Polym. Sci. B Polym. Phys.* **1989**, *27*, 723–741. [[CrossRef](#)]
35. Senanayake, K.K.; Fakhrabadi, E.A.; Liberatore, M.W.; Mukhopadhyay, A. Diffusion of Nanoparticles in Entangled Poly(vinyl alcohol) Solutions and Gels. *Macromolecules* **2019**, *52*, 787–795. [[CrossRef](#)]
36. Wu, C.-S. *Handbook of Size Exclusion Chromatography and Related Techniques: Revised and Expanded*; CRC Press: Boca Raton, FL, USA, 2003; Volume 91.
37. Dorgan, J.R.; Williams, J.S. Melt rheology of poly(lactic acid): Entanglement and chain architecture effects. *J. Rheol.* **1999**, *43*, 1141–1155. [[CrossRef](#)]
38. Akamatsu, M. Hydrophobicity of chemical compounds including pesticides in the environment. *J. Environ. Sci. Sustain. Soc.* **2021**, *10*, 27–30. [[CrossRef](#)]
39. Kunstche, J.; Horst, J.C.; Bunjes, H. Cryogenic transmission electron microscopy (cryo-TEM) for studying the morphology of colloidal drug delivery systems. *Int. J. Pharm.* **2011**, *417*, 120–137.
40. Shimanouchi, T.; Hayashi, T.; Toramoto, K.; Fukuma, S.; Hayashi, K.; Yasuhara, K.; Kimura, Y. Microfluidic and hydrothermal preparation of vesicles using sorbitan monolaurate/polyoxyethylene (20) sorbitan monolaurate (Span 20/Tween 20). *Colloids Surf. B* **2021**, *205*, 111836. [[CrossRef](#)]
41. Guo, F.; Chen, B. Numerical study on Taylor bubble formation in a micro-channel T-junction using VOF method. *Microgravity Sci. Technol.* **2009**, *21*, S51–S58. [[CrossRef](#)]
42. Ayrilmis, N. Effect of fire retardants on surface roughness and wettability of wood plastic composites panels. *BioResources* **2011**, *6*, 3178–3187. [[CrossRef](#)]
43. Ma, M.; Hill, R.M. Superhydrophobic surfaces. *Curr. Opin. Colloid Interface Sci.* **2006**, *11*, 193–202. [[CrossRef](#)]
44. Xu, J.; Li, M.; Zhao, Y.; Lu, Q. Control over the hydrophobic behavior of polystyrene surface by annealing temperature based on capillary template wetting method. *Colloids Surf. A* **2007**, *302*, 136–140. [[CrossRef](#)]
45. Marmur, A. The Lotus Effect: Superhydrophobicity and Metastability. *Langmuir* **2004**, *20*, 3517–3519. [[CrossRef](#)] [[PubMed](#)]

Disclaimer/Publisher’s Note: The statements, opinions and data contained in all publications are solely those of the individual author(s) and contributor(s) and not of MDPI and/or the editor(s). MDPI and/or the editor(s) disclaim responsibility for any injury to people or property resulting from any ideas, methods, instructions or products referred to in the content.